

CrossMark
click for updatesCite this: *J. Anal. At. Spectrom.*, 2015, 30, 1207Received 17th October 2014
Accepted 2nd February 2015

DOI: 10.1039/c4ja00349g

www.rsc.org/jaas

UV-light microscope: improvements in optical imaging for a secondary ion mass spectrometer†

Noriko T. Kita,* Peter E. Sobol, James R. Kern, Neal E. Lord and John W. Valley

A large radius secondary ion mass spectrometer (SIMS) has been used for *in situ* stable isotope analyses of geological samples at the scale of 1–10 μm . However, the original reflected light microscope of the CAMECA IMS 1280 SIMS had an optical resolution of ~ 3.5 μm , which made it difficult to accurately position the analytical beam on the sample at the μm scale. We modified the optical microscope to use ultraviolet (UV) light illumination and UV compatible optical components, keeping the same mechanical design inside the vacuum chamber. The optical resolution was improved to 1.3 μm with the UV-light microscope system. In addition, we wrote Badgerscope®, a LabVIEW based software for sample imaging, which greatly enhanced the accuracy of positioning and efficiency of instrument operation. These improvements can be adapted to other micro-beam instruments where complex optical paths may be imposed by instrument design.

Introduction

A large radius secondary ion mass spectrometer (SIMS) has been used for stable isotope analyses of geological samples at high precision and accuracy.^{1,2} Isotope analyses are performed by sputtering of the sample surface using Cs^+ or O^- primary ions that are focused, typically, to a diameter of 10–15 μm ; secondary ions ejected from the sample surface are extracted to the mass spectrometer. Using the CAMECA IMS 1280 at the University of Wisconsin-Madison (WiscSIMS Laboratory), we have developed high precision stable isotope analysis techniques using primary beam sizes as small as 1–2 μm .^{3,4} However, positioning of the analysis location on the sample surface using such a small primary beam was very difficult because the original reflected light microscope of the IMS 1280 had an optical resolution of ~ 3.5 μm , which did not allow the operator to see the 1–2 μm -size SIMS pits produced by sputtering of the sample surface (Fig. 1a). As a consequence of this limitation, small-spot analyses at WiscSIMS were performed as traverses of spots 2 or 3 μm apart by moving the sample in one direction (Fig. 1b) and the exact locations were confirmed after SIMS analysis using scanning electron microscopy (SEM). Even with a large analysis spot size of 10 μm , the low-resolution optical image leads to positioning errors, such as analysis spots that overlap with an adjacent mineral phase or the epoxy resin used for mounting grains, that result in inaccurate data. CAMECA IMS-series instruments could be equipped with a

secondary electron detector to image secondary electrons produced from the sample surface by the sputtering of finely focused (<1 μm) Cs^+ primary ions. However, geological samples are often electrical insulators and require an electron-gun for charge compensation that prevents use of a secondary electron detector. In addition, secondary electron imaging does not work if the instrument is tuned with a positive secondary ion beam.

The resolution of the reflected light microscope of the first IMS 1280 instrument, which was delivered to WiscSIMS in 2005, is determined by the geometry of the optical microscope, the optical characteristics of its components, and the wavelength spectra of the white-light source. It is difficult to modify the microscope geometry because of space constraints in the main chamber that contains multiple high-voltage components. Alternatively, optical resolution would be improved by using shorter wavelength and/or monochromatic light. Here, we report modification of the optical microscope system of the IMS 1280 using a UV-light source. We replaced multiple optical components to make them UV compatible, but did not make any changes to the mechanical design of optics inside the vacuum chamber. In addition, we wrote a LabVIEW-based software package for sample imaging.

Modification of the optical microscope system

IMS 1280 reflected-light microscope system

The optical microscope system consists of three components: (1) an illuminator outside of the vacuum chamber, (2) a reflected light microscope inside the vacuum, and (3) a zoom lens and a CCD (charge-coupled device) camera outside of the vacuum (Fig. 2). The illuminator unit is placed outside of the

WiscSIMS, Department of Geoscience, University of Wisconsin-Madison, 1215 W. Dayton St., Madison, WI 53706, USA. E-mail: noriko@geology.wisc.edu

† Electronic supplementary information (ESI) available. See DOI: 10.1039/c4ja00349g

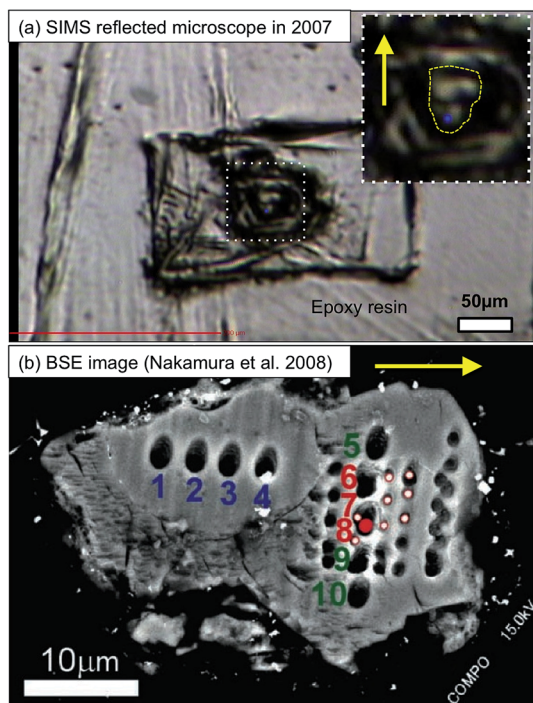


Fig. 1 An example of the images obtained with the original reflected light microscope of a CAMECA IMS 1280 for a particle from the Wild 2/81P comet sampled by the NASA Stardust Mission. (a) Reflected light microscope image of the particle "Gozen-sama" (C2081,1,108,1) during SIMS analysis in 2007. The enlarged view of the dotted square is shown in the inset at the right-top corner, which includes the particle that is outlined by a dashed line. The blue dot in the center indicates the position of SIMS analyses. (b) High resolution back-scattered electron image of the same particle after the SIMS analyses (Nakamura *et al.*⁴). Analyses were made as two traverses of 2 μm spots (numbered 1–10) and a 6 \times 6 grid of 1 μm spots. Filled red and white dots correspond to the locations of 2 μm and 1 μm spot analyses, respectively, that show a large mass-independent isotope anomaly in ^{16}O . During the grid analysis, backlash of the sample stage stepping motors resulted in significant overlap between the first and second traverses (right end), as well as for the first and second spots of every traverse (*i.e.*, 6 spots look like only 5 spots). (b) is rotated CW relative to (a); the yellow arrows indicate the orientation of the particle.

main chamber, which includes a halogen lamp for white light illumination, a condenser lens for focusing light on the sample surface, and an adjustable angle mirror for illuminating the sample surface with an incidence angle of 30° from normal. The optical microscope unit of the IMS 1280 is enclosed behind the extraction plate of the secondary ion optics, which is located 5 mm from the sample surface. The microscope unit consists of an optical waveguide enclosed within the extraction plate, an objective lens, a mirror, and a transfer lens. The microscope is also positioned 30° from normal to the sample surface opposite the angle of the illuminator. The position of the objective lens along the optical axis is adjusted by manually rotating a knob that is connected to the microscope unit *via* an UHV (ultra high vacuum) mechanical feedthrough. There is a shutter placed in front of the waveguide to avoid deposits on the surface of the waveguide from material sputtered from the sample. The field of view is 450 μm \times 380 μm at maximum magnification of the

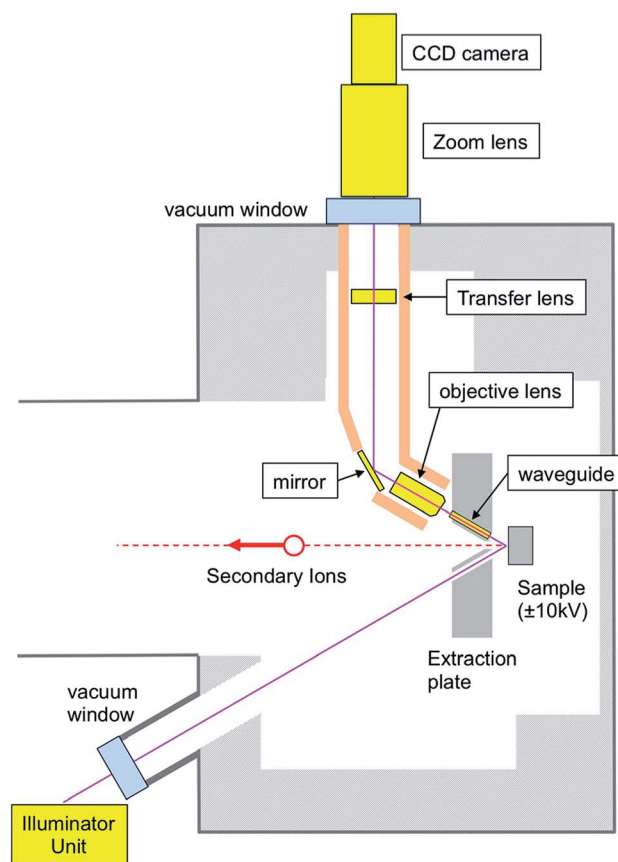


Fig. 2 Schematic diagram of the reflected light microscope system of a CAMECA IMS 1280. Names in the boxes are parts that were replaced for the UV-light microscope system. Illumination light source, zoom lens, and camera are located outside of the vacuum chamber. Illuminator unit is not shown in detail. See main text for a detailed description.

zoom lens. Because of the angled view, the image is reduced in the Y-direction relative to X to 87% (cosine of 30°) and shows defocusing in the Y direction on either side of the center line. The originally supplied color CCD camera image with 752 (horizontal, H) \times 582 (vertical, V) pixels was captured by the graphics board of the PC and displayed using CAMECA software. One pixel of the image corresponded to 0.60 μm (H) \times 0.67 μm (V) on the sample at maximum magnification, though effective resolution may be degraded by the factor of two (~ 1.2 μm) because of interpolating a color filter array (typically a unit of four pixels for red, green, and blue) on the CCD.

Blue LED light source

We first replaced the white-light source with a monochromatic blue ($\lambda \sim 455$ nm) light emitting diode (LED) without replacing any other optical components. We replaced the illuminator assembly (designed by the Physical Science Laboratory, University of Wisconsin; PSL) to adapt to a star configuration LED, which is described on the WiscSIMS website (<http://www.geology.wisc.edu/~wiscsims/>). With this change to a shorter, monochromatic light, the optical resolution was

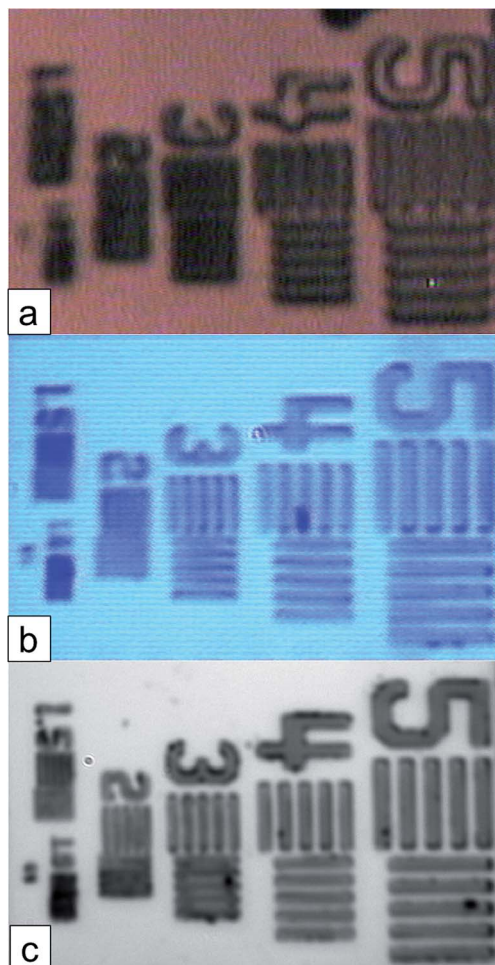


Fig. 3 Reflected light microscope images of a resolution-calibration target, CAMECA SIMS test sample. Numbers next to each set of lines (1.0 to 5) indicate width and distance between lines in micro-meters. Resolution of an image corresponds to the minimum width of lines that can be resolved. (a) Original CAMECA IMS 1280 microscope image with white light source. Resolution $\sim 3.5 \mu\text{m}$. Full color image. (b) Modification to blue-LED-light source (455 nm). Resolution $\sim 2.2 \mu\text{m}$. Blue color image. (c) UV-light microscope system using LED-light source (365 nm). Resolution $\sim 1.3 \mu\text{m}$. Monochrome image.

improved so that $3 \mu\text{m}$ lines of a resolution-calibration target were clearly resolved (Fig. 3b), which could not be resolved in the original system (Fig. 3a). As a trade-off with spatial resolution, this approach lost the color information of the sample surface. However, color information is less important than the sharpness of the images because most of our geological specimens are coated either by gold or carbon. Sample navigation is made by identification of surface geometric features, such as cracks, pits, and differing surface textures, that are compared to the detailed images taken from SEM or optical microscopes before the samples are loaded into the SIMS.

UV-light microscope system

Subsequently, we modified the illumination to use a high power (700 mW) 365 nm UV-light LED source. Several optical

components that did not transmit UV light were replaced with UV compatible versions, including the optical waveguide, the objective lens, the mirror and the transfer lens inside the vacuum chamber; as well as the condenser lens of the illuminator and the zoom lens below the CCD camera that are outside of the vacuum chamber. The same illumination assembly was used as for the blue-LED-light source. The original CCD camera was replaced with a UV-sensitive CCD camera capable of high definition images (1380×1040 pixels). With this camera, one pixel of the image corresponds to $0.33 \mu\text{m}$ (H) \times $0.38 \mu\text{m}$ (V) on the sample surface. These replacement components are listed in Table 1. We note that the original mirror was a conventional back-surface mirror and transmitted UV light to a limited extent, but was replaced by a UV-compatible front-surface mirror. With the original mirror, double reflections of the UV light were observed that disappeared after replacement with the front-surface mirror. It seems that a small amount of light was reflected at the non-coated front surface of the original mirror, which was enhanced when using the UV light due to its shorter wavelength. The double reflection images were displaced by a few μm vertically, which degraded optical resolution significantly. As shown in Fig. 3c, the $2 \mu\text{m}$ lines of the resolution-calibration target are now resolved and the $1.5 \mu\text{m}$ lines are resolved in the horizontal direction.

LED light sources have higher requirements for heat dissipation, but at the same time require less space than a conventional halogen lamp. The smaller space requirements allow a further redesign of the illuminator optics. The redesign will improve the heat dissipation from the LED while reducing the length and complexity of the optical path. This will improve the efficiency of transmission of light from the LED into the vacuum chamber.

Badgerscope© sample viewing software

We wrote Badgerscope©, a new LabVIEW-based imaging software package, to incorporate image manipulation because the new CCD camera is not compatible with the CAMECA software and the PC interface provided with the instrument. The new software has additional functionality compared to the original CAMECA software, which provides improved accuracy and efficiency of targeting samples (see detail in ESI-1†). Badgerscope© consists of an image window to show CCD camera images with two targeting marks for analysis positions (Fig. S1 in ESI-1†). One of the marks is used as a reference point that is set at the beginning of each analysis session to show the location of the primary beam. Another mark is used to navigate sample stage positions (-10 mm to $+10 \text{ mm}$ in X and Y) by communicating with the CAMECA software. It is possible to freely change the shape and position of these marks to accurately reflect the actual beam. Badgerscope© allows improved signal/noise in images through variable image averaging, enhanced images through manipulation of brightness and contrast and the use of false color. It also has a “difference” function that displays the difference between a live image and a reference image, allowing subtle changes to be detected, such as those made by a short duration exposure of the primary beam to

Table 1 List of components replaced for the UV-light microscope system

Components	Part numbers or material used
Light source	LED Engin LZ1-10U600
Illuminator condenser lens	CAMECA 91480823
Waveguide	UV-grade fused silica rod Tower Optical 4520-0162
Objective lens assembly	CAMECA 91480827
Mirror	Edmonds Optics 68-316
Transfer lens assembly	CAMECA 91480826
Zoom lens	Pentax B2528-UV lens
HD camera	JAI CM-140GE-UV

the sample surface (Fig. 4). This function is very useful for small and low intensity primary beams, which sputter the sample surface very slowly and leave pits that cannot otherwise be easily identified.

Comparison between blue and UV-light illumination

The optical resolutions of blue-LED and UV-light microscope systems are estimated using the edge of a feature with a sharp boundary ($<0.1 \mu\text{m}$) on the resolution-calibration target (Fig. 3). The estimated resolution, defined as the distance where the intensity changes by 50%, is $2.2 \mu\text{m}$ for the blue LED using the original microscope system and $1.3 \mu\text{m}$ for the UV-light

microscope system. These values are consistent with the resolution-calibration target images in Fig. 3b and c, respectively. We compare two images of the resolution-calibration targets illuminated by the blue LED and the UV-light LED using the same UV-light microscope system (Fig. S2, ESI-2[†]). Blue-LED illumination on the new UV-light microscope system resolved $2 \mu\text{m}$ lines, but not $1.5 \mu\text{m}$ lines (Fig. S2, ESI-2[†]), which indicates that the optical resolution is between $1.5 \mu\text{m}$ and $2 \mu\text{m}$. These data indicate that the optical resolution is improved both by the replacement of the optical system and the illumination source.

The maximum resolution (d) of an optical microscope system is given by $d \sim 0.5\lambda/\text{NA}$, where λ and NA are the wavelength of light and numerical aperture, respectively. Applying $\text{NA} = 0.12$ for the IMS 1280 microscope system, d is estimated to be $1.8 \mu\text{m}$ and $1.5 \mu\text{m}$, for blue-LED and UV-light illumination, respectively. These values are comparable to the estimated optical resolution using resolution-calibration targets. In addition to the improvements related to shorter wavelength, there are other factors that improved the final resolution of the new system. The original color camera operated at lower resolution with an effective pixel size corresponding to $\sim 1.2 \mu\text{m}$ on the sample surface. The new higher resolution monochrome camera in the UV-light microscope system has an effective pixel size measuring $0.3\text{--}0.4 \mu\text{m}$ on the sample surface, so that the camera does not limit the optical resolution. Replacement of the front-surface mirror resulted in clear and sharp images without double reflections (Fig. S2, ESI-2[†]). Although the geometric designs of optical components are the same as in the original system, the replaced UV-grade optical components may have higher optical quality, which may further reduce the various aberrations.

Advantage of angled illumination

The angled illumination and camera view of the IMS 1280 microscope system results in defocusing of the sample image in the Y axis away from the center. This is a disadvantage in viewing the sample image with the larger field of view of medium magnification ($\sim 800 \mu\text{m} \times 500 \mu\text{m}$), though it is not significant within the field of view at maximum magnification ($450 \mu\text{m} \times 380 \mu\text{m}$). The defocusing effect along the Y direction is not changed with the new UV-light microscope system (Fig. S3, ESI-2[†]). The angled view on the IMS 1280 has advantages in acquiring reliable stable isotope measurements. Topography of the sample surface may degrade accuracy of stable isotope analyses because a tilted surface deforms the surface potential ($\pm 10 \text{ kV}$) where secondary ions are ejected. Kita *et al.*² recommended that surface topography of samples should be less than $3 \mu\text{m}$ in order to obtain accurate results. Although we inspect the topography of each sample mount prior to SIMS analysis, edges of grains sometimes show small amounts of topography. The angled illumination of the IMS 1280 optical microscope system is very sensitive to surface topography compared to normal-incidence illumination. The heterogeneous brightness of the sample surface would indicate surface topography is significant. We can determine the beam position on the sample for reliable analysis guided by reflected-light illumination with the improved optical resolution.

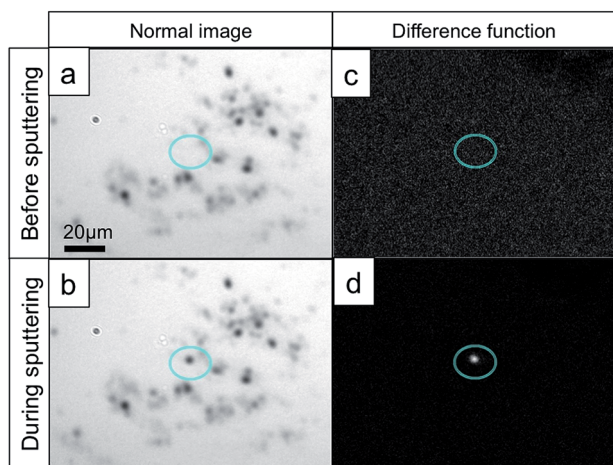


Fig. 4 Example of the “difference function” in the Badgerscope[©] software. Four images are shown on the slightly pitted surface of a Si-wafer. (a) Normal microscope image of sample surface before sputtering, showing numerous dots and shadows in similar size and brightness to small SIMS spots. Brightness and contrast are optimized. Blue oval is a marker to navigate sample stage motions. (b) Normal microscope image after sputtering with a small SIMS spot ($\sim 2 \mu\text{m}$ Cs^+ beam). The position of SIMS spot is identified (inside blue oval) by comparing images (a) and (b). (c) Image using the difference function before sputtering starts. The image shows only a black background because the live-image does not change from the original image in (a). (d) Image using the difference function during sputtering. A bright spot appears within a few seconds at the location where the primary beam hits the sample due to subtle changes of brightness.

Application of the new UV-light microscope system to SIMS analysis

Alignment of the primary beam

One of the important aspects of SIMS analysis is tuning the primary beam for intensity and size that is optimized for a research goal. The primary-beam size is typically 10–15 μm for stable isotope analysis, but should be small enough that the beam does not overlap multiple phases. Overlap of the beam with different minerals would result in a mixed analysis and erroneous instrumental bias corrections. Even within a single mineral grain, geological specimens are often zoned in chemistry and isotope ratios that correspond to distinct events or environments in geologic time and space, so that primary beam size should ideally be smaller than the dimensions of the zoning. However, the primary beam current commonly decreases with approximately the square of beam diameter, which results in poorer precision of isotope ratio measurements due to lower secondary ion intensities. Therefore, the analyst must optimize intensity and beam-spot size for each analysis session in order to maximize the scientific value of the analysis. The distribution of primary beam intensities within a given

primary beam spot is also important. In the case of oxygen isotope ratio measurements of Ca carbonate, reproducibility of the calcite standard degraded if the primary beam is better focused (Gaussian beam) and makes a deeper sputter crater. Rastering the primary beam during the analysis would produce flatter crater shape, though it would enlarge the size of analysis spot.

Primary beam alignment is generally performed by illuminating secondary ions from a homogeneous material (such as a Si-wafer) using direct ion imaging. The secondary ions are projected onto the multi-channel plate (MCP) at the end of the secondary ion path, showing the size, shape, and density distribution of the primary beam. However, the lateral resolution of the direct ion image is relatively poor (\sim a few μm) when apertures and slits of the mass spectrometer are fully opened to achieve high secondary ion transmission (\sim 90%). The new UV-light microscope allows us to evaluate the size and density distribution of the primary beam more easily by optically imaging craters sputtered in a clean Si wafer (Fig. 5a). The Badgerscope[®] software makes various kinds of false color images (Fig. 5b), which can be used to vary the contrast differences so as to enhance observation of the heterogeneity of primary beam density within a primary beam spot.

Application to paleoclimate research

Fig. 6 shows an example of SIMS analysis of a planktic foraminifer that employs oxygen isotope ratios to distinguish the primary foraminifera calcite shell from secondary diagenetic crystallites.⁶ Conventional stable isotope analysis of whole shells of foraminifera would produce erroneous results due to contamination by diagenetic calcite. Prior to SIMS analysis, secondary electron (SE) imaging of the sample was conducted so as to assist navigation between analysis positions. The SE images show surface features, such as cracks and topography, consistent with the reflected light image. True paleoclimate signatures are preserved only in the thin chamber wall (\leq 10 μm thickness), which can be analyzed using 3 μm SIMS spots. The new UV-light microscope shows clearly the location of the thin chamber wall so that the analyst can precisely separate the chamber wall and diagenetic cement for analysis. The results of SIMS analysis have been used to confirm a global temperature rise at the Paleocene–Eocene boundary⁶ (55.8 million years ago).

Beyond optical resolution

The analysis of samples using a beam size of 2 $\mu\text{m} \times$ 1 μm is much easier with UV-light than white light illumination because it is possible to see the SIMS pits during analysis. These small pits were not visible with the original viewing system. However, accurate positioning of the beam requires care because the beam size and the optical resolution are comparable. Nakashima *et al.*⁷ developed a new targeting procedure that combines Focused Ion Beam (FIB) milling to delicately remove the surface coating of a 1 $\mu\text{m} \times$ 1 μm target area, which can then be viewed using SIMS secondary ion imaging with a scanning sub- μm primary beam (Fig. 7). The new UV-light microscope with improved optical resolution were necessary for

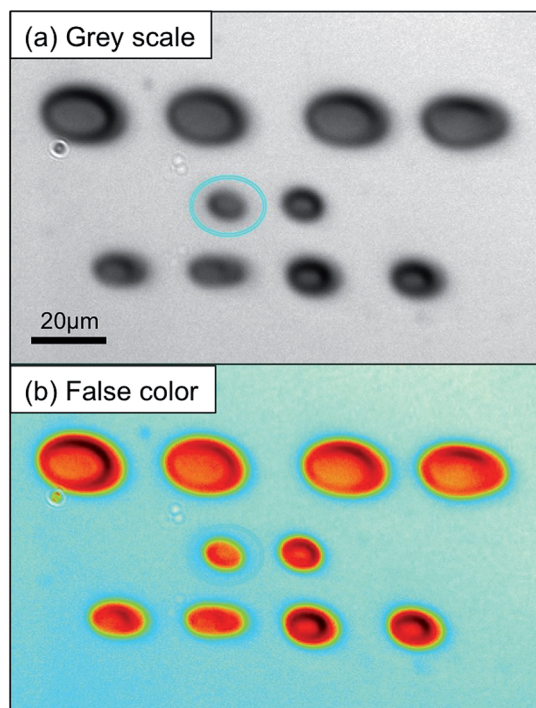


Fig. 5 The UV-light microscope images of primary beam spots on a clean Si-wafer. The example shows primary beam spots with various sizes and shapes when O^- primary ions were aligned for Köhler illumination conditions.⁵ (a) Normal grey scale image with optimized brightness and contrast. (b) False-color image, which shows surface topography of sputtered craters. Sizes and shapes of individual spots differ due to changes in aperture size and parameters of the primary ion column, which are examined by observing spots on a Si-wafer using the UV-light microscope. The primary beam parameters are chosen to optimize the primary beam conditions.

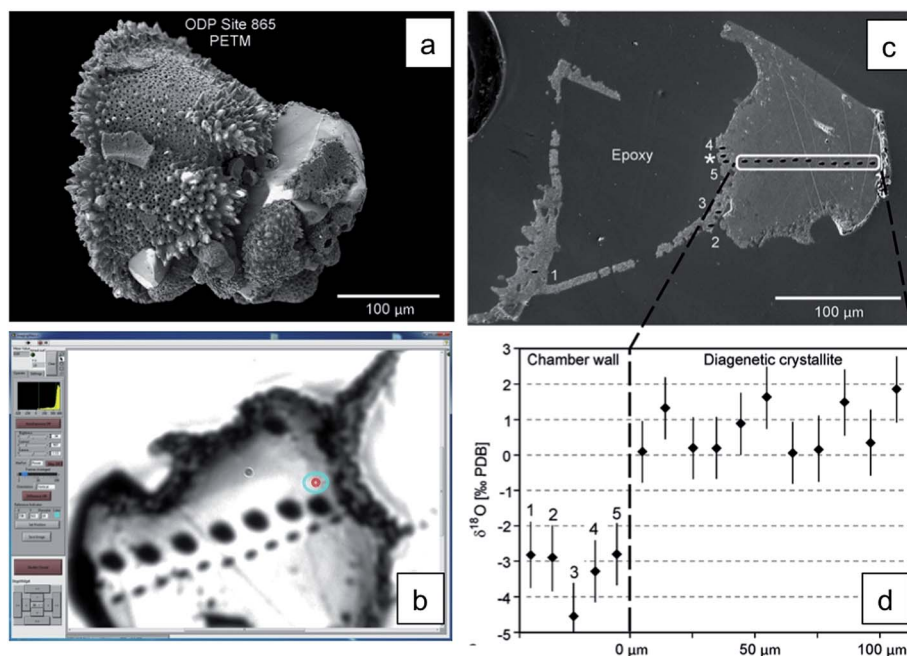


Fig. 6 Oxygen isotope analyses of a foraminifera and diagenetic cement from an Ocean Drilling Program core sample (Kozdon *et al.*⁶). (a) Scanning electron (SE) image of the shell of a planktic foraminifer before mounting in epoxy resin. (b) The UV-light microscope image of the cross section after SIMS analysis (field of view ~ 150 μm). Two parallel traverses of 10 μm and 3 μm SIMS spots are shown. (c) SE image of the same cross section after 3 μm spot analyses. Thin chamber walls of the foraminifer (spot numbers 1–5) were accurately aimed using the UV-light microscope. (d) Oxygen isotope analyses of the foraminifera and cement with 3 μm spots. Paleoclimate isotope signatures are only recorded in the thin chamber wall and could not be studied without a small beam spot. Accurate aiming of these spots required UV-light illumination.

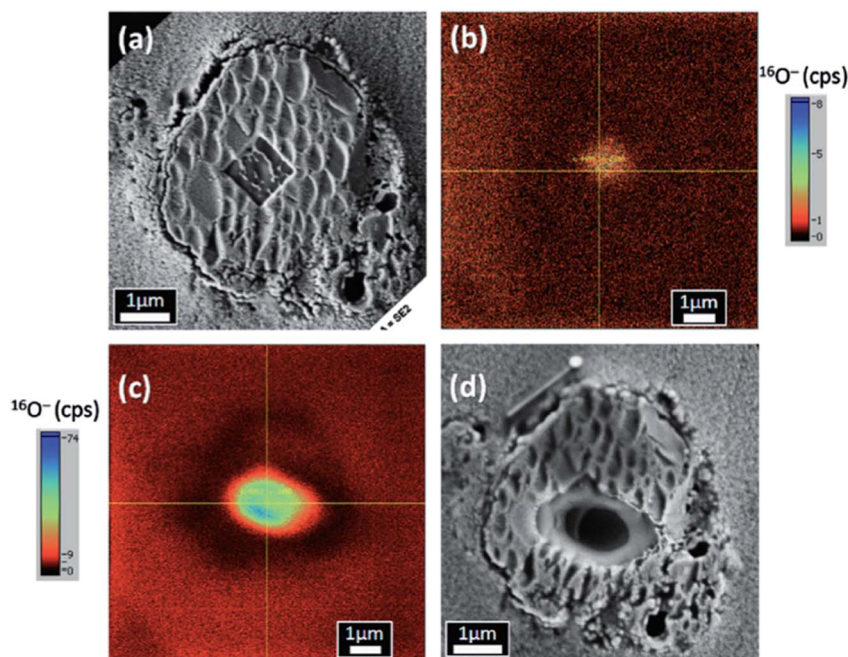


Fig. 7 FIB marking technique for aiming of a SIMS analysis target at sub- μm accuracy (Nakashima *et al.*⁷). (a) SEM image of the Wild 2 particle (Track 77 fragment 4; 4 $\mu\text{m} \times 4 \mu\text{m}$) with 1 μm square FIB mark where surface carbon coating was removed. The particle has a nm-scale irregular surface from microtome slicing during sample preparation. (b) The scanning ion image ($^{16}\text{O}^-$) of the particle before oxygen isotope analysis using finely focused (≤ 1 μm) primary beam across a 10 $\mu\text{m} \times 10 \mu\text{m}$ area, showing the FIB mark with high secondary O^- signals. (c) The scanning ion image of the particle after SIMS analysis using a 2 $\mu\text{m} \times 1 \mu\text{m}$ spot. (d) SEM image of the particle with SIMS spot at the center.

locating the specimen for secondary ion imaging (Fig. 7b). Using this technique, it is possible to aim and hit small specimens with a reproducibility of 0.5 μm . As a result, Nakashima *et al.*⁷ analyzed the center of comet particles as small as 2 μm \times 4 μm , which could not be done previously during a study by Nakamura *et al.*⁴ The accurate targeting of small particles is important for precious space-mission return-particle analyses, such as the Stardust Mission where a majority of the particles collected are much smaller than 10 μm .⁸

Summary

We have modified the reflected-light microscope system of a CAMECA IMS 1280 SIMS using UV-light illumination and compatible optical components. These changes improved spatial resolution when viewing samples from ~ 3.5 μm to ~ 1.3 μm . The new Badgerscope© software improved our positioning accuracy and efficiency, which contributes greatly to the quality of SIMS analyses. Using the secondary ion imaging technique, we achieved positioning accuracy as good as 0.5 μm . A similar modification using a UV-light illumination source would be applicable to the optical microscope system of other instruments such as an electron microprobe when there are limitations of mechanical re-design, but need for better imaging resolution.

Acknowledgements

This work is supported by the NSF-EAR Instrumentation and Facilities Program (EAR-0744079, -1053466, -1355590). Part of the engineering design and the determination of optical properties of the original microscope optical components were made by Ken Kriesel and Dan Wahl under contract with the Physical Sciences Laboratory, University of Wisconsin. We thank John Craven (Edinburgh University) for loan of CAMECA 4f optical

microscope components, and Emmanuel De Chambost, Fabrice Le Duigou, and Paula Peres (CAMECA Instruments) for technical assistance and advice. Reinhard Kozdon kindly provided the image of a foraminifera sample by UV-light microscope. Constructive comments by anonymous referees improved the clarity of the manuscript. We also thank to Daisuke Nakashima, Takayuki Ushikubo, Kouki Kitajima, and colleagues in the WiscSIMS laboratory for helpful suggestions and assistance for the project.

References

- 1 J. W. Valley and N. T. Kita, *Mineral. Assoc. Can., Short Course Ser.*, 2009, **41**, 19–63.
- 2 N. T. Kita, T. Ushikubo, B. Fu and J. W. Valley, *Chem. Geol.*, 2009, **264**, 43–57.
- 3 F. Z. Page, T. Ushikubo, N. T. Kita, L. R. Riciputi and J. W. Valley, *Am. Mineral.*, 2007, **92**, 1772–1775.
- 4 T. Nakamura, T. Noguchi, A. Tsuchiyama, T. Ushikubo, N. T. Kita, J. W. Valley, M. E. Zolensky, Y. Kakazu, K. Sakamoto, E. Mashio, K. Uesugi and T. Nakano, *Science*, 2008, **321**, 1664–1667.
- 5 N. T. Kita, T. Ushikubo, K. B. Knight, R. A. Mendybaev, A. M. Davis, F. M. Richter and J. H. Fournelle, *Geochim. Cosmochim. Acta*, 2012, **86**, 37–51.
- 6 R. Kozdon, D. C. Kelly, K. Kitajima, A. Strickland, J. H. Fournelle and J. W. Valley, *Paleoceanography*, 2013, **28**, 517–528.
- 7 D. Nakashima, T. Ushikubo, D. J. Joswiak, D. E. Brownlee, G. Matrajt, M. K. Weisberg, M. E. Zolensky and N. T. Kita, *Earth Planet. Sci. Lett.*, 2012, **357–358**, 355–365.
- 8 D. E. Brownlee, D. J. Joswiak and G. Matrajt, *Meteorit. Planet. Sci.*, 2012, **47**, 453–470.